Soft Matter

PAPER

View Article Online
View Journal | View Issue

Cite this: *Soft Matter*, 2025, **21**, 4622

Optothermally induced active and chiral motion of colloidal structures†

Rahul Chand,* Ashutosh Shukla, Sneha Boby and G. V. Pavan Kumar *

Artificial soft matter systems have proven to be important tools to harness mechanical motion for microscale manipulation. Typically, this motion is driven either by external fields or by mutual interactions between the colloids. In the latter scenario, dynamics arise from non-reciprocal interactions among colloids within a chemical environment. In contrast, we eliminate the need for a chemical environment by utilizing a large area of optical illumination to generate thermal fields. The resulting optothermal interactions introduce non-reciprocity to the system, enabling active motion of the colloidal structure. Our approach involves two types of colloids: passive and thermally active. The thermally active colloids contain absorbing elements that capture energy from the incident optical beam, creating localized thermal fields around them. In a suspension of these colloids, the thermal gradients generated drive nearby particles through attractive thermo-osmotic forces. We investigate the resulting dynamics, which lead to various swimming modes, including active propulsion and chiral motion. We have also simulated the dynamics of the colloidal structures by solving the coupled Langevin equations to gain insight into the emerging motion. By exploring the interplay between optical forces, thermal effects, and particle interactions, we aim to gain insights into controlling colloidal behavior in non-equilibrium systems. This research has significant implications for directed self-assembly, microfluidic manipulation, and the study of active matter.

Received 14th November 2024,
Accepted 3rd May 2025

DOI: 10.1039/d4sm01348d

rsc.li/soft-matter-journal

Introduction

Out-of-equilibrium soft matter systems display a range of complex behaviors including active propulsion,[1–12] self-organization,[13–15] and other emergent dynamics.[16–20] These phenomena arise as a result of the mutual interaction between the individual element and external stimuli.[21,22] Artificial synthetic colloidal systems provide a controlled test bed for studying this behavior.[23] Various external fields such as optical,[24–32] chemical,[28,29,33] electrical[34–38] and magnetic fields[37–40] are commonly used as manipulation techniques. Most of the studies are based on inherently asymmetric systems where the structural or compositional asymmetry induces force imbalance leading to the active motion of the structure.[25,41–48]

In contrast, researchers have proposed the use of symmetrical colloids with different chemical reactivities to enable active motion without inherent asymmetry.[49–54] In these cases, the dynamics of the colloidal structures are powered by non-reciprocal interactions. However, these methods require chemical environments such as hydrogen peroxide[49] or water–lutidine mixtures.[50,51] Such requirements restrict the usability of these platforms.

Regarding this, some recent studies have shown that in an aqueous medium, colloidal particles can be dragged to the heat center by the thermo-osmotic slip flow produced by it.[55–57] One can utilize this process to harness non-reciprocal attractive interactions without any chemical environment. In systems with absorbing and non-absorbing colloids, these interactions induce imbalance and drive the motion.[58] Recently, we have reported the directional motion obtained through such thermo-osmotic interactions in various optical confinements (such as Gaussian, line, and ring beam).[58,59] The interaction between the absorbing and non-absorbing colloids fuels the dynamics. However, the induction of similar dynamics in an unconfined environment is yet to be explored in detail. These may have widespread applications in areas such as directed self-assembly,[60] microfluidic manipulation,[61–64] and the exploration of non-equilibrium processes in active matter.[65]

Motivated by this, in this article, we experimentally investigated the dynamics of colloidal structures made of absorbing thermally active (A) and non-absorbing passive (P) colloids under broad-area optical illumination (see Fig. 1(a)). In a suitable large area, with uniform optical illumination, the gradient optical forces are insignificant and the optical field only enables selective heating of the colloidal particles depending on their absorbing

Department of Physics, Indian Institute of Science Education and Research (IISER) Pune, Pune, 411008, India. E-mail: rahul.chand@students.iiserpune.ac.in, pavan@iiserpune.ac.in

† Electronic supplementary information (ESI) available. See DOI: https://doi.org/10.1039/d4sm01348d

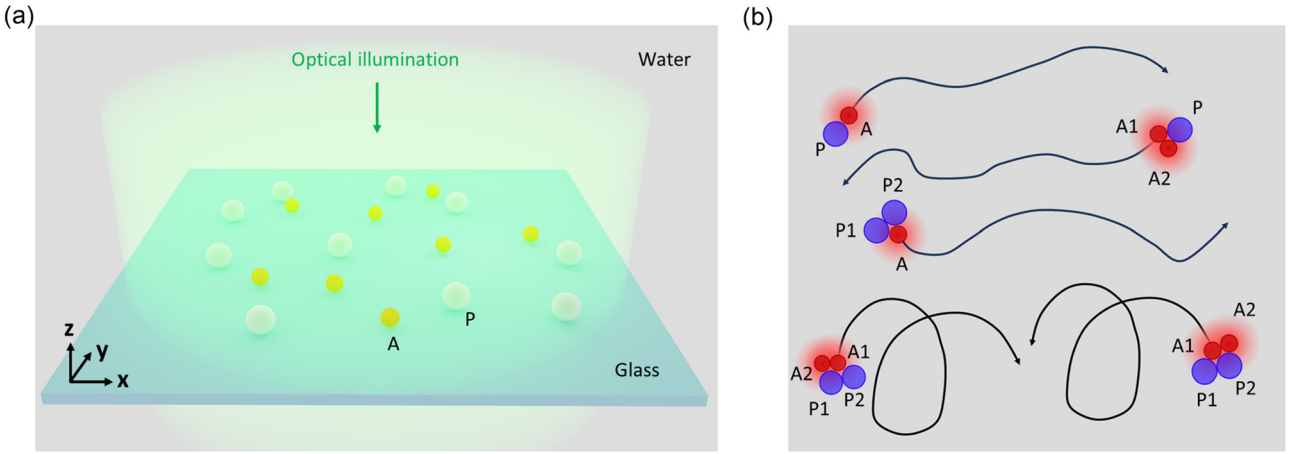

Fig. 1 Schematic of the dynamics. (a) When an aqueous colloidal suspension of thermally active (A) and passive (P) colloids is illuminated by a large optical field, the thermally active colloids absorb the laser energy and heat up. This results in a temperature difference between the colloids. (b) The temperature difference induces thermo-osmotic interactions between the colloids. As a result, different colloidal structures, such as dimers, trimers, and quadromers, are formed, and they exhibit various swimming modes.

characteristics. Thus, such illumination generates temperature gradients without any confinement potential. We examine how these temperature gradients affect particle motion and interactions, leading to different swimming modes (see Fig. 1(b)). Our simulation results support these findings. In our study, we used the optically generated thermal field instead of its chemical counterpart because it is measurable and controllable as a result of various recent advancements.[66] In addition, optothermal interactions provide promising applications for micromanipulation and self-assembly in various other emergent phenomena.[67–71]

Experimental method

The colloidal particles used in our experiment are melamine formaldehyde (MF) colloids of diameter 2 μm as passive (P) colloids and nano-particulate iron–oxide infused polystyrene (PS) colloids of diameter 1.3 μm as thermally active (A) colloids. These colloids are obtained from microParticles GmbH. The calculated absorption and scattering cross-sections of these colloidal particles are shown in Supplementary information 1 (ESI†). We used a dilute aqueous suspension of these colloids in our sample cell. As shown in Fig. 2(a), a dual-channel optical microscopy setup is used for the experiments. A 532 nm continuous-wave Gaussian laser beam was coupled to the sample plane using a 50×, 0.5 NA objective lens. Since our laser diode provides limited optical output (<120 mW), the low power output of our laser diode limits the ability to create an appropriate, large area of uniform optical illumination. Thus, we employed a defocused optical beam instead of optical plane wave illumination. For that, the sample plane was positioned away from the objective lens's focal plane (F, dashed line in Fig. 2(a)). Additionally, a white light source was integrated into the setup *via* a beam splitter to facilitate visualization of the dynamics. Most of the experiments are performed with a laser power of 45 mW at the back aperture of the objective lens, and the illumination extent in the sample plane is $\simeq$32 μm diameter leading to an optical intensity of 56 μW μm^{-2} in the sample plane. The intensity of the optical illumination can be altered by changing the power of the laser beam or by modulating the extent of the defocused beam. To ensure that under such optical illumination, the colloidal systems do not experience a lot of variation in intensity over their trajectory, we have considered the shorter experimental trajectories, approximately 10 μm. Within such a span of the trajectories, the intensity variation experienced by the colloidal system is <18%. If we consider a longer span of the trajectories, then the intensity variation will be significant, and the role of direct optical forces cannot be ruled out. The image of the sample plane is then collected using a 50×, 0.8 NA objective lens and then projected onto a CCD/fast camera sensor. The CCD/fast camera captures the dynamics at a rate of 30/500 frames per second. The trajectories of the colloidal particles were extracted from the recorded video files using the TrackMate[72] extension of Fiji software.[73]

Results and discussion

Active motion of the dimer structure

Under such optical illumination, thermally active colloids effectively harness laser energy and dissipate heat. Typically, in the water medium, the transient heating of the system occurs on the timescale of microseconds. The temperatures reach a steady state at the timescales relevant to our study. This process generates a localized temperature distribution around the thermally active colloids. This thermal field results in thermo-osmotic slip fluid flow, which acts as an environmental cue to manipulate the motion of nearby colloidal particles. Specifically, when the thermally active colloids interact with their passive counterpart, these thermo-osmotic interactions become non-reciprocal, forming various bound structures. The simplest possibility is a dimer structure composed of one thermally active (A) and passive (P) colloid. Due to the non-reciprocity of the interactions, these dimer structures exhibit propulsion behavior as illustrated in the trajectory depicted

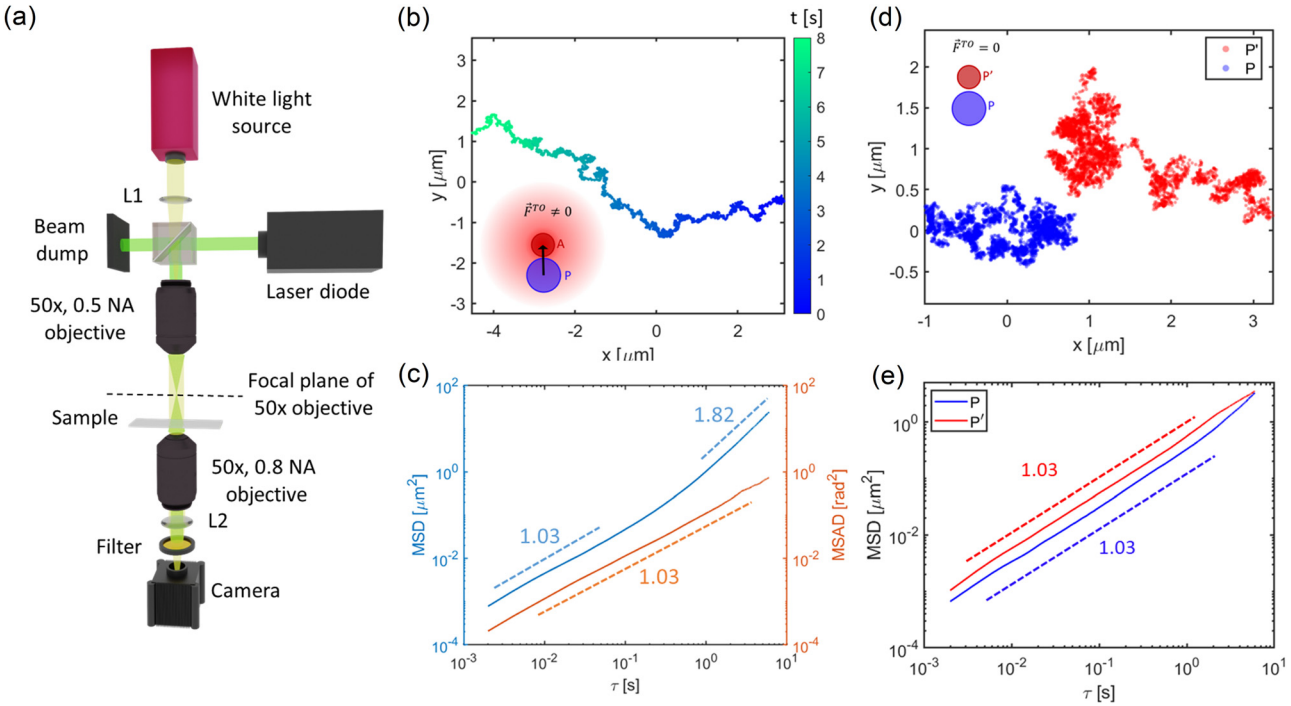

Fig. 2 Dynamics of a colloidal dimer under optical illumination. (a) Experimental setup. Under defocused optical illumination, the thermally active (A) colloid gets heated more than the passive (P) colloids. This temperature difference between the colloids induces an attractive thermo-osmotic $\left(\vec{F}^{TO}\right)$ interaction between them, leading to the formation of an active dimer (AD) structure. (b) The trajectory of the centroid of this active dimer structure is shown. The corresponding orientation vector of the structure is illustrated by the black arrow in the inset. (c) The mean squared displacement (MSD) and the mean squared angular displacement (MSAD) of the orientation vector of the active dimer structure. The MSD indicates a diffusive followed by a ballistic trend, whereas the MSAD shows a diffusive trend over the experimental time scale. (d) The trajectory of a dimer structure when the thermally active colloid (A) is replaced by a passive colloid (P′) of the same composition and size. In this case, due to the absence of heating, the thermo-osmotic interaction is not present, resulting in random diffusion of the colloids. (e) The corresponding linear scaling of the MSD of individual colloids indicates the role of the thermo-osmotic interaction in the formation of AD and the resulting active propulsion.

in Fig. 2(b). We have calculated the mean-squared displacement (MSD) to quantify these dynamics, as presented in Fig. 2(c). The MSD analysis reveals a diffusive followed by a ballistic motion within our experimental timescale. The ballistic behavior is emblematic of typical active systems.[74] Generally, active structures exhibit three different timescales in MSD: diffusive behavior and ballistic behavior, followed by diffusive behavior with increasing lagtime (τ) (for details, see Supplementary information 2, ESI†). The large time-scale diffusive behavior generally appears beyond the rotational diffusive time scale τ_r of the colloidal particles, which is generally of the order of 10^2 s. Since, in our case, the experimental time duration is $\simeq$10 s, in our experimental MSD, we do not observe the large time scale diffusive behavior.

Furthermore, we can associate a specific orientation direction with this active dimer structure, represented by a black arrow connecting the centers of the two colloids as shown in the inset of Fig. 2(b). To investigate how the orientation of this active dimer structure evolves, we estimated the mean squared angular displacement (MSAD) of this directional vector, as shown in Fig. 2(c). Slope 1 suggests that the orientation of the active dimer lacks any inherent rotational bias. In contrast, if we replace the thermally active colloid with a passive colloid (P′) of the same composition and size, then no tightly bound dimer structure exhibiting active motion is formed. The colloids exhibit independent diffusive motion, as can be seen from Fig. 2(d) (also see the ESI,† Video S1). The calculated MSD of the individual colloids, in Fig. 2(e), scales linearly with the lagtime, further emphasizing the colloids' unbiased Brownian motion. This observation suggests the vital role of slip flow-induced non-reciprocal attractive interactions in enabling the activity. We note that the dimer structure propels without any additional chemical environment.

Inducing rotational bias

To gain deeper insights into the dynamics that emerge from evolving colloidal structures due to temperature differences, we experimentally studied the dynamics of trimer and quadromer structures. There are two distinct configurations, AT1 and AT2. (i) AT1 contains one thermally active colloid (A1) paired with two passive colloids (P1) and (P2) and (ii) AT2 contains two thermally active colloids (A1) and (A2) alongside one passive colloid (P1). In both these trimer configurations, the non-reciprocal thermo-osmotic interaction can only lead to an imbalance of effective force along the structure's symmetry line. As a result, both of them exhibit propulsion behavior similar to the active dimer structure (see the ESI,† Video S2). Fig. 3(a) and (b) show the corresponding time-evolving trajectories of these two trimer configurations. We can clearly observe from the trajectory that

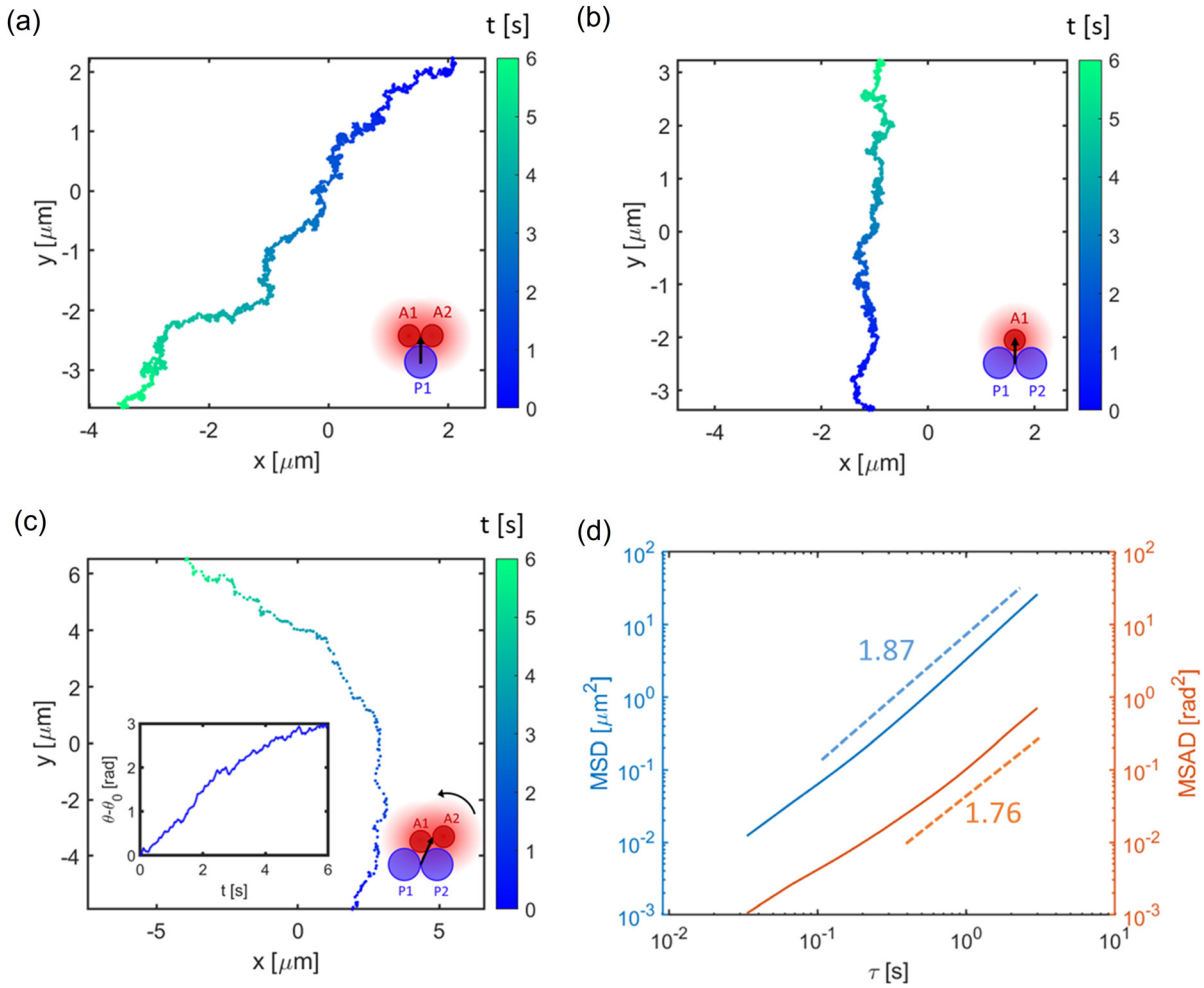

Fig. 3 Dynamics of active trimer and quadromer structures and the emergence of chirality. Two possible trimer configurations are (a) containing one passive (P1) with two thermally active colloids (A1) and (A2) and (b) two passive (P1) and (P2) with one thermally active colloid (A1). The trajectories of both these trimer configurations indicate only active propulsion without any preferred chirality or handedness. (c) In contrast, the active quadromer structures composed of two passive (P1) and (P2) and two thermally active colloids (A1) and (A2) exhibit anticlockwise handedness based on the arrangement of the constituent colloids. The corresponding time evolution of the orientation vector for active quadromers is shown in the inset. (d) The MSD and MSAD indicate the activity signature in both linear and angular coordinates.

although these trimer structures undergo active propulsion, they also do not show any preferred angular motion (see Supplementary information 3, ESI†).

In contrast, if we consider a quadromer structure composed of two passive and thermally active colloids (as shown in Fig. 3(c)), due to the respective arrangement of the colloids, passive colloid P1 is relatively more distant than passive colloid P2 from thermally active colloid A2. This leads to different magnitudes of attractive thermo-osmotic force acting on the passive colloids. The thermo-osmotic force on P2 is greater than that on P1. As a result, P2 tends to move faster than P1. But since the quadromer moves together, the trajectory tends to move toward colloid P1, resulting in a tendency of anticlockwise chiral motion, as depicted in Fig. 3(c) (also see the ESI,† Video S2). Since our optical illumination is within a limited spatial extent, we experimentally did not observe a full curling trajectory. We have recorded the dynamics with a 30 fps CCD camera. We can define an orientation vector of the colloidal quadromer along the line joining from the center of mass of passive colloids P1 and P2 to the center of mass of thermally active colloids A1 and A2. The time evolution of the orientation vector clearly indicates the persistent angular motion in the case of chiral quadromers, as indicated in the inset of Fig. 3(c). The calculated MSD and MSAD for such a chiral quadromer structure are shown in Fig. 3(d). In contrast to the active dimer and trimer structure, in this case, we observed a ballistic trend in both the MSD and the MSAD. Similar chiral motion is also observed in natural active systems[75–78] and artificial colloidal systems with inherent asymmetry mostly in chemical environments.[24,42,50,79–83] But here, we show the dynamics in symmetric colloids with a non-chemical environment purely due to the optothermal interaction.

To understand the influence of thermo-osmotic interactions in the active and chiral motion, we have simulated the dynamics of the colloidal structures as given below.

Simulation of the dynamics of the colloidal structures

To simulate the dynamics of the colloids due to the temperature difference, we considered thermally active (A) and passive (P) colloids of diameters 1.3 μm and 2 μm, respectively. To model the absorbing nature of the thermally active colloids, we considered that they are at a higher temperature compared to their passive counterparts. In such a situation, the dynamics of colloid i will be determined using the Langevin equation given by

$$\gamma_i \vec{v}_i = \vec{F}_i^{\text{ext}} + \sqrt{2k_B T_i \gamma_i} \vec{\zeta}_i, \tag{1}$$

where $\vec{v}_i$ and γ_i are the instantaneous velocity and viscous drag coefficient of colloid i. The last term $\sqrt{2k_B T_i \gamma_i}\vec{\zeta}_i$ is the stochastic noise-induced random force term, where k_B is the Boltzmann constant and T_i is the temperature of colloid i. All other forces are considered in the external force term $\vec{F}_i^{\text{ext}}$. Details of these forces are given below.

The large area optical field is modeled as plane wave illumination. This idealized the optical field as infinitely extended in simulation, in contrast to the experiments with a limited illumination region. In such a situation, no confining gradient optical force acts on the colloids (see Supplementary information 4, ESI†). Besides, the scattering optical force on the colloids acts in the propagation direction that pushes the colloids towards the bottom glass coverslip (see Supplementary information 4, ESI†). Due to the collective effect of gravity and the scattering optical forces, the dynamics of the colloids become two-dimensional. Since there is no in-plane component of the optical forces, we have not considered any optical force in our two dimensional simulation. The optical field is only used to create temperature differences between the colloids, which further harnesses temperature-mediated interactions between them. Secondary optical interactions between the colloids, such as optical binding, may play some role. However, the thermo-osmotic flow-induced forces are dominant within our experimental parameters, as can be seen from Supplementary information 5 (ESI†).

Being at an elevated temperature ($T_A = T_s + \Delta T$) compared to the surroundings, the thermally active colloids set up a thermal field in the surrounding medium as given by

$$T(r > a_A) = \Delta T \frac{a_A}{r} + T_s, \tag{2}$$

where a_A is the radius of the thermally active colloid and T_s is the ambient temperature. Such thermal fields produced by thermally active colloids induce thermo-osmotic slip fluid flow at the glass water interface. If the j-th colloid is a thermally active colloid, the thermo-osmotic slip flow produced by it can be written as

$$\vec{v}_j = \frac{\chi}{T_s} \vec{\nabla} T_j, \tag{3}$$

where χ is the slip coefficient of the glass surface. This slip flow can drag the nearby colloids to heated thermally active colloids. The corresponding drag force ($\vec{F}_{ij}^{\text{TO}}$) on colloid i due to colloid j can be written as

$$\vec{F}_{ij}^{\text{TO}} = \gamma_i \vec{v}_j. \tag{4}$$

Since the passive colloids cannot generate thermo-osmotic slip flow on their own, they cannot induce thermo-osmotic force on the other colloids. In contrast, passive colloids can feel drag due to the thermo-osmotic flow produced by thermally active colloids. Thus, thermo-osmotic drag force $\vec{F}_{ij}^{\text{TO}} = 0$, if j = passive colloids, and $\vec{F}_{ij}^{\text{TO}} = \gamma_i \vec{v}_j \neq 0$, if j = thermally active colloids.

In addition to the above-mentioned forces, we have also considered the Lennard Jones forces ($\vec{L}J_{ij}$) between the colloids to ensure the exclusion region for one colloid due to the presence of the others. These $\vec{L}J_{ij}$ forces acting on colloid i due to the presence of colloid j can be written as

$$\vec{L}J_{ij} = 4\varepsilon \left(12\frac{\sigma^{12}}{r_{ij}^{13}} - 6\frac{\sigma^6}{r_{ij}^7} \right) \hat{r}_{ij}, \tag{5}$$

where $\sigma = a_i + a_j$ and ε is the Lennard Jones parameter. a_i, a_j and r_{ij} are the radius of colloids i, j and the distance between them. $\hat{r}_{ij}$ is the unit vector along the position of colloid i with respect to colloid j.

Taking the above-mentioned forces into account, the coupled Langevin equations involving passive and thermally active colloids can be written as

$$\gamma_i \vec{v}_i = \sum_{j \neq i} \vec{L}J_{ij} + \sum_{j \neq i} \vec{F}_{ij}^{\text{TO}} + \sqrt{2k_B T_i \gamma_i} \vec{\zeta}_i. \tag{6}$$

For a dimer structure composed of one thermally active (A) and passive (P) colloid, the above coupled Langevin equations will be reduced to

$$\vec{v}_A = \frac{d\vec{r}_A}{dt} = \frac{1}{\gamma_A} \left(\vec{L}J_{A,P} + \sqrt{2k_B T_A \gamma_A} \zeta_A \right), \tag{7a}$$

$$\vec{v}_P = \frac{d\vec{r}_P}{dt} = \frac{1}{\gamma_P} \left(\vec{L}J_{P,A} + \vec{F}_{P,A}^{\text{TO}} + \sqrt{2k_B T_P \gamma_P} \zeta_P \right). \tag{7b}$$

Solving these coupled Langevin equations, one can simulate the dynamics of active dimer structures (see the ESI,† Video S3). We have used the following parameters in our simulation based on previous experimental studies: $\varepsilon = 20 \times 10^{-21}$ J, $\chi = 1.87 \times 10^{-9}$ m^2 s^{-1}, $\gamma_A = 1.7 \times 10^{-8}$ and $\gamma_P = 4.0 \times 10^{-8}$ N s m^{-1}.[59] In Fig. 4(a), a simulated trajectory of such an active dimer structure is shown for $\Delta T = 2$ K. The corresponding MSD and MSAD of the active dimer structure are shown in Fig. 4(b). One can clearly observe the diffusive to ballistic followed by a diffusive transition in the MSD, whereas the MSAD shows only diffusive behaviors. Similarly, one can solve the Langevin equation for the active trimer and quadromer structures and study their dynamics (see the ESI,† Video S4). The trajectories of the two possible trimer structures are shown in Fig. 4(c) and (d), respectively. The corresponding MSD and MSAD are shown in Supplementary information 3 (ESI†). They also exhibit qualitatively similar behavior to the active dimer structures. In contrast, the active quadromer structures clearly indicate a preferred handedness. The trajectories and the time evolution of the orientation vector of two such quadromer structures with opposite handedness are shown in Fig. 4(e) (see the ESI,† Video S5). The calculated MSD and MSAD of the active quadromer structure (Fig. 4(f)) clearly indicate the diffusive to ballistic followed by the diffusive behavior. The long-time diffusive behavior in the MSAD is due to the stochastic noise,

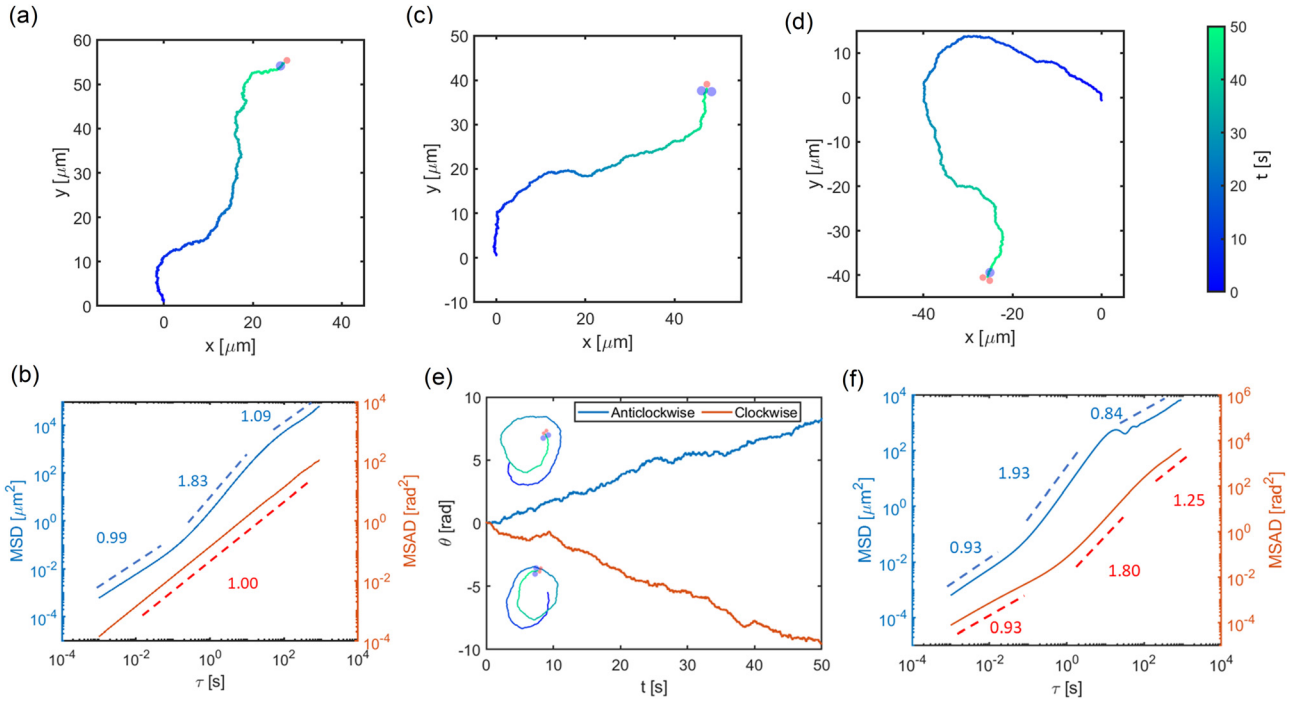

Fig. 4 Simulated dynamics of the colloidal structures. (a) The simulated trajectory of a dimer structure composed of one passive and one thermally active colloid. (b) The calculated average MSD of the dimer structure clearly shows a diffusive to ballistic followed by a diffusive trend. In contrast, the MSAD is diffusive throughout the whole timescale. The active trimer structures' corresponding time-evolving trajectories are shown in (c) and (d). (e) The trajectories of the active quadromers, along with the time-evolving orientation vector, clearly indicate that the quadromers exhibit specific handedness. (f) The corresponding calculated MSD and MSAD of the quadromer structure indicate the activity signature in both the position and angular scale.

the relative arrangement of the colloidal particles changes, and the quadromer switches from one-handedness to another-handedness in an unbiased manner (see the ESI,† Video S6). We have also compared the simulated and experimental MSD time scale values in Supplementary information 6 (ESI†).

Control over the dynamics

In the previous sections, we have shown how the temperature difference between the colloids and the resulting thermo-osmotic interaction leads to active propulsion and chiral motion in different colloidal structures. In this section, we experimentally try to understand the role of the intensity of the incident optical field and the size of the colloidal constituents in the dynamics of colloidal structures. Fig. 5(a) shows the velocity of the active dimer and trimer structure at various laser intensities. The thermal field and the thermo-osmotic interaction between the colloids can be controlled using the intensity of the incident optical field. We have also observed a similar trend in simulation (see Supplementary information 7, ESI†). One can also tune the dynamics by changing the constituent colloids' size. Fig. 5(b)

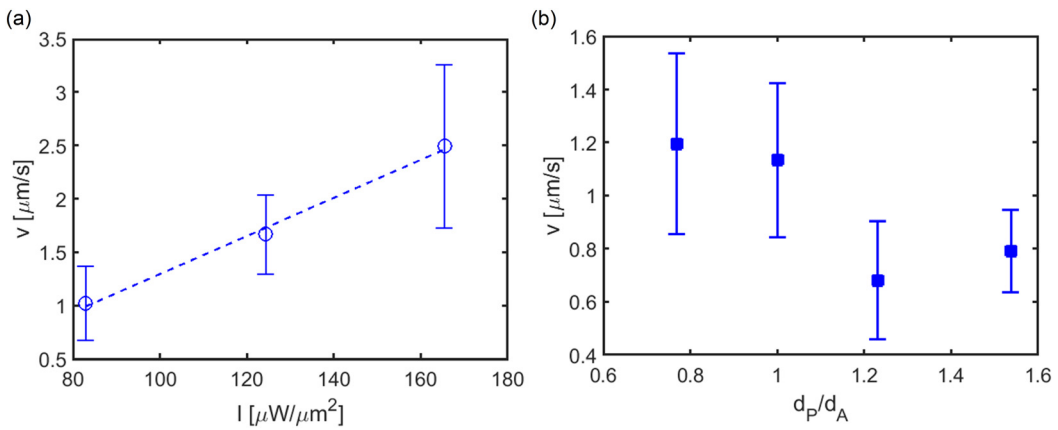

Fig. 5 Control over the dynamics of active dimer structures. An incremental trend of the linear velocities (v) of the active dimer (AD) as a function of laser intensity (I). The dashed lines indicate the linear fit. (b) The velocity (v) of the active dimer structure as a function of the diameter of passive colloids shows a decremental trend with increasing diameter of the passive colloids.

shows the active velocity of the dimer structures as a function of the ratio of the diameter of the passive to thermally active colloids. In this case, we have only changed the passive colloid's diameter d_P = 1, 1.3, 1.6, 2 μm, keeping the diameter of the thermally active colloid fixed (d_A = 1.3 μm). Since the thermally active colloid is unchanged, the extent of heating and thermo-osmotic fluid flow remains unchanged, and the variation of the velocity is due to the passive colloid. The velocity shows a decreasing trend with increasing diameter of the passive colloid. A qualitatively similar trend is also observed in simulation (see Supplementary information 8, ESI†).

Conclusions

Thus, in this study, we have experimentally explored the intricate behaviors of colloidal structures composed of thermally active and passive colloids. Our investigation revealed various emergent swimming modes, including active propulsion and chiral handedness. Such dynamics are primarily driven by temperature differences between the constituent colloids, resulting from an attractive nonreciprocal interaction between the colloids, as we found that these emerging dynamics are absent when the non-reciprocal attractive interactions are ignored.

In contrast to the available literature, we did not rely on any chemical environment, such as hydrogen peroxide or 2,6-lutidine, to harness the nonreciprocal interaction.[49–53] In our study, the non-reciprocal interaction between the colloids is employed by the thermo-osmotic slip fluid flow due to the temperature difference of the colloids. These interactions result in an inherent force imbalance within the structures, leading to both propulsion and chiral motion influenced by the constituent colloidal particles. Additionally, we observed that the dynamics of the colloidal structures can be enhanced or diminished by tuning the magnitude of the temperature mismatch, achievable through the intensity of optical illumination. We have also solved Langevin equations to validate the active dynamics of colloidal structures resulting from temperature differences between colloids.

In addition, since the dynamics emerge due to thermo-osmotic flow produced by the heated colloid in an aqueous solution, this platform is potentially useful for cargo transport. This study may also contribute valuable insights into the dynamics of colloidal structures, paving the way for potential applications in micro-engineering[84–86] and microfluidic devices.[61–64]

Author contributions

R. C., A. S., and G. V. P. K. designed the study. R. C., A. S., and S. B. performed the experiments and analysis. A. S. has helped in the Brownian dynamics simulations. R. C. wrote the manuscript draft. All the authors reviewed the manuscript.

Data availability

All the data including the simulation logic and experimental validation along with the analysis are included in the manuscript and ESI.†

Conflicts of interest

There are no conflicts to declare.

Acknowledgements

R. C. thanks Diptabrata Paul and Sumant Pandey for the fruitful discussion. This work was partially funded by AOARD (grant number FA2386-23-1-4054) and the Swarnajayanti fellowship grant (DST/SJF/PSA-02/2017-18) to G. V. P. K.

Notes and references

1 É. Fodor, C. Nardini, M. E. Cates, J. Tailleur, P. Visco and F. Van Wijland, *Phys. Rev. Lett.*, 2016, **117**, 038103.
2 T. Speck, *Europhys. Lett.*, 2016, **114**, 30006.
3 S. C. Takatori and J. F. Brady, *Phys. Rev. E*, 2015, **91**, 032117.
4 M. J. Bowick, N. Fakhri, M. C. Marchetti and S. Ramaswamy, *Phys. Rev. X*, 2022, **12**, 010501.
5 D. Needleman and Z. Dogic, *Nat. Rev. Mater.*, 2017, **2**, 1–14.
6 J. Van der Gucht, Grand challenges in soft matter physics, *Front. Phys.*, 2018, **6**, 87.
7 O. Hallatschek, S. S. Datta, K. Drescher, J. Dunkel, J. Elgeti, B. Waclaw and N. S. Wingreen, *Nat. Rev. Phys.*, 2023, **5**, 407–419.
8 G. De Magistris and D. Marenduzzo, *Phys. A: Stat. Mech. Appl.*, 2015, **418**, 65–77.
9 É. Fodor and M. C. Marchetti, *Phys. A: Stat. Mech. Appl.*, 2018, **504**, 106–120.
10 S. Ramaswamy, *Annu. Rev. Condens. Matter Phys.*, 2010, **1**, 323–345.
11 T. Sanchez, D. T. Chen, S. J. DeCamp, M. Heymann and Z. Dogic, *Nature*, 2012, **491**, 431–434.
12 C. Weber, P. K. Radtke, L. Schimansky-Geier and P. Hänggi, *Phys. Rev. E: Stat., Nonlinear, Soft Matter Phys.*, 2011, **84**, 011132.
13 T. H. Tan, A. Mietke, J. Li, Y. Chen, H. Higinbotham, P. J. Foster, S. Gokhale, J. Dunkel and N. Fakhri, *Nature*, 2022, **607**, 287–293.
14 D. P. Singh, U. Choudhury, P. Fischer and A. G. Mark, *Adv. Mater.*, 2017, **29**, 1701328.
15 N. A. Araújo, L. M. Janssen, T. Barois, G. Boffetta, I. Cohen, A. Corbetta, O. Dauchot, M. Dijkstra, W. M. Durham and A. Dussutour, *et al.*, *Soft Matter*, 2023, **19**, 1695–1704.
16 E. O. Budrene and H. C. Berg, *Nature*, 1995, **376**, 49–53.
17 Q. Yang, M. Jiang, F. Picano and L. Zhu, *Nat. Commun.*, 2024, **15**, 2874.
18 A. Curatolo, N. Zhou, Y. Zhao, C. Liu, A. Daerr, J. Tailleur and J. Huang, *Nat. Phys.*, 2020, **16**, 1152–1157.
19 E. B. Steager, C.-B. Kim and M. J. Kim, *Phys. Fluids*, 2008, **20**, 073601.
20 L. Theeyancheri, S. Chaki, T. Bhattacharjee and R. Chakrabarti, *Phys. Rev. Res.*, 2024, **6**, L012038.
21 T. Speck, *Soft Matter*, 2020, **16**, 2652–2663.
22 S. C. Takatori and J. F. Brady, *Soft Matter*, 2014, **10**, 9433–9445.
23 W. Wang, X. Lv, J. L. Moran, S. Duan and C. Zhou, *Soft Matter*, 2020, **16**, 3846–3868.

24 X. Peng, Z. Chen, P. S. Kollipara, Y. Liu, J. Fang, L. Lin and Y. Zheng, *Light: Sci. Appl.*, 2020, **9**, 141.
25 T. Raj, S. Roy, A. Kumar, B. Roy, E. Mani and S. Sudhakar, *J. Colloid Interface Sci.*, 2025, **677**, 986–996.
26 S. Nedev, S. Carretero-Palacios, P. Kühler, T. Lohmüller, A. S. Urban, L. J. Anderson and J. Feldmann, *ACS Photonics*, 2015, **2**, 491–496.
27 G. Tkachenko, V. G. Truong, C. L. Esporlas, I. Sanskriti and S. Nic Chormaic, *Nat. Commun.*, 2023, **14**, 1691.
28 S. Simoncelli, J. Summer, S. Nedev, P. Kühler and J. Feldmann, *Small*, 2016, **12**, 2854–2858.
29 I. Buttinoni, G. Volpe, F. Kümmel, G. Volpe and C. Bechinger, *J. Phys.: Condens. Matter*, 2012, **24**, 284129.
30 A. Haldar, S. B. Pal, B. Roy, S. D. Gupta and A. Banerjee, *Phys. Rev. A: At., Mol., Opt. Phys.*, 2012, **85**, 033832.
31 R. N. Kumar, A. D. Ranjan, S. Roy, S. D. Gupta, N. Ghosh and A. Banerjee, *Phys. Rev. A*, 2024, **110**, 023512.
32 B. Roy, N. Ghosh, S. Dutta Gupta, P. K. Panigrahi, S. Roy and A. Banerjee, *Phys. Rev. A: At., Mol., Opt. Phys.*, 2013, **87**, 043823.
33 P. Kumar, L. Theeyancheri and R. Chakrabarti, *Soft Matter*, 2022, **18**, 2663–2671.
34 L. Zhang and Y. Zhu, *Langmuir*, 2012, **28**, 13201–13207.
35 S. Erez, E. Karshalev, Y. Wu, J. Wang and G. Yossifon, *Small*, 2022, **18**, 2101809.
36 Y.-L. Chen, C.-X. Yang and H.-R. Jiang, *Sci. Rep.*, 2018, **8**, 5945.
37 A. F. Demirörs, M. T. Akan, E. Poloni and A. R. Studart, *Soft Matter*, 2018, **14**, 4741–4749.
38 Y. Komazaki, H. Hirama and T. Torii, *J. Appl. Phys.*, 2015, **117**, 154506.
39 P. Tierno, R. Golestanian, I. Pagonabarraga and F. Sagués, *Phys. Rev. Lett.*, 2008, **101**, 218304.
40 P. Tierno, R. Golestanian, I. Pagonabarraga and F. Sagués, *J. Phys. Chem. B*, 2008, **112**, 16525–16528.
41 H. Moyses, J. Palacci, S. Sacanna and D. G. Grier, *Soft Matter*, 2016, **12**, 6357–6364.
42 H.-R. Jiang, N. Yoshinaga and M. Sano, *Phys. Rev. Lett.*, 2010, **105**, 268302.
43 L. Wang, M. N. Popescu, F. Stavale, A. Ali, T. Gemming and J. Simmchen, *Soft Matter*, 2018, **14**, 6969–6973.
44 M. M. Stanton, J. Simmchen, X. Ma, A. Miguel-López and S. Sánchez, *Adv. Mater. Interfaces*, 2016, **3**, 1500505.
45 J. Simmchen, J. Katuri, W. E. Uspal, M. N. Popescu, M. Tasinkevych and S. Sánchez, *Nat. Commun.*, 2016, **7**, 10598.
46 F. Kümmel, B. Ten Hagen, R. Wittkowski, I. Buttinoni, R. Eichhorn, G. Volpe, H. Löwen and C. Bechinger, *Phys. Rev. Lett.*, 2013, **110**, 198302.
47 A. Mondal, B. Roy and A. Banerjee, *Opt. Express*, 2015, **23**, 8021–8028.
48 L. Theeyancheri, S. Chaki, N. Samanta, R. Goswami, R. Chelakkot and R. Chakrabarti, *Soft Matter*, 2020, **16**, 8482–8491.
49 T. Yu, P. Chuphal, S. Thakur, S. Y. Reigh, D. P. Singh and P. Fischer, *Chem. Commun.*, 2018, **54**, 11933–11936.
50 F. Schmidt, B. Liebchen, H. Löwen and G. Volpe, *J. Chem. Phys.*, 2019, **150**, 094905.
51 J. Grauer, F. Schmidt, J. Pineda, B. Midtvedt, H. Löwen, G. Volpe and B. Liebchen, *Nat. Commun.*, 2021, **12**, 6005.
52 A. Varma, T. D. Montenegro-Johnson and S. Michelin, *Soft Matter*, 2018, **14**, 7155–7173.
53 J. Codina, H. Massana-Cid, P. Tierno and I. Pagonabarraga, *Soft Matter*, 2022, **18**, 5371–5379.
54 S. Kumar, M. Gunaseelan, R. Vaippully, A. Kumar, M. Ajith, G. Vaidya, S. Dutta and B. Roy, *Biomed. Opt. Express*, 2020, **11**, 3555–3566.
55 A. P. Bregulla, A. Würger, K. Günther, M. Mertig and F. Cichos, *Phys. Rev. Lett.*, 2016, **116**, 188303.
56 M. Fränzl and F. Cichos, *Nat. Commun.*, 2022, **13**, 656.
57 D. Quinn and F. Cichos, *Front. Nanotechnol.*, 2023, **5**, 1135408.
58 R. Chand, C. E. Rani, D. Paul and G. V. P. Kumar, *ACS Photonics*, 2023, **10**, 4006–4013.
59 R. Chand, A. Shukla and G. V. P. Kumar, *ACS Photonics*, 2025, **12**, 855–863.
60 S. E. Chung, W. Park, S. Shin, S. A. Lee and S. Kwon, *Nat. Mater.*, 2008, **7**, 581–587.
61 K. Jae-Sung and J. H. Oh, *Appl. Sci.*, 2018, **8**, 992.
62 S. Hettiarachchi, H. Cha, L. Ouyang, A. Mudugamuwa, H. An, G. Kijanka, N. Kashaninejad, N.-T. Nguyen and J. Zhang, *Lab Chip*, 2023, **23**, 982–1010.
63 M. Rhee and M. A. Burns, *Lab Chip*, 2008, **8**, 1365–1373.
64 T. M. Schneider, S. Mandre and M. P. Brenner, *Phys. Rev. Lett.*, 2011, **106**, 094503.
65 L. K. Davis, K. Proesmans and É. Fodor, *Phys. Rev. X*, 2024, **14**, 011012.
66 M. Fränzl, S. Muinos-Landin, V. Holubec and F. Cichos, *ACS Nano*, 2021, **15**, 3434–3440.
67 P. S. Kollipara, Z. Chen and Y. Zheng, *ACS Nano*, 2023, **17**, 7051–7063.
68 Y. Liu and A. W. Poon, *Opt. Express*, 2010, **18**, 18483–18491.
69 J. H. Shin, J. Seo, J. Hong and S. K. Chung, *Sens. Actuators, B*, 2017, **246**, 415–420.
70 S. Ghosh, A. Biswas, B. Roy and A. Banerjee, *Soft Matter*, 2019, **15**, 4703–4713.
71 C. Bechinger, R. Di Leonardo, H. Löwen, C. Reichhardt, G. Volpe and G. Volpe, *Rev. Mod. Phys.*, 2016, **88**, 045006.
72 J.-Y. Tinevez, N. Perry, J. Schindelin, G. M. Hoopes, G. D. Reynolds, E. Laplantine, S. Y. Bednarek, S. L. Shorte and K. W. Eliceiri, *Methods*, 2017, **115**, 80–90.
73 J. Schindelin, I. Arganda-Carreras, E. Frise, V. Kaynig, M. Longair, T. Pietzsch, S. Preibisch, C. Rueden, S. Saalfeld and B. Schmid, *et al.*, *Nat. Methods*, 2012, **9**, 676–682.
74 G. Volpe, S. Gigan and G. Volpe, *Am. J. Phys.*, 2014, **82**, 659–664.
75 B. Vincenti, G. Ramos, M. L. Cordero, C. Douarche, R. Soto and E. Clement, *Nat. Commun.*, 2019, **10**, 5082.
76 E. Lauga, W. R. DiLuzio, G. M. Whitesides and H. A. Stone, *Biophys. J.*, 2006, **90**, 400–412.
77 K. Ērglis, Q. Wen, V. Ose, A. Zeltins, A. Sharipo, P. A. Janmey and A. Cēbers, *Biophys. J.*, 2007, **93**, 1402–1412.

78 C. N. Dominick and X.-L. Wu, *Biophys. J.*, 2018, **115**, 588–594.
79 B. Liebchen and D. Levis, *Europhys. Lett.*, 2022, **139**, 67001.
80 F. Schmidt, A. Magazzù, A. Callegari, L. Biancofiore, F. Cichos and G. Volpe, *Phys. Rev. Lett.*, 2018, **120**, 068004.
81 L. Caprini, H. Löwen and U. M. B. Marconi, *Soft Matter*, 2023, **19**, 6234–6246.
82 P. L. Muzzeddu, H. D. Vuijk, H. Löwen, J.-U. Sommer and A. Sharma, *J. Chem. Phys.*, 2022, **157**, 134902.
83 M. Donato, A. Mazzulla, P. Pagliusi, A. Magazzù, R. Hernandez, C. Provenzano, P. Gucciardi, O. Maragò and G. Cipparrone, *Sci. Rep.*, 2016, **6**, 31977.
84 B. Xu, Y. Zhao, X. Chen, R. Fu, H. Li, S. Xie, H. Liu, Y. Li, S. Zhang and B. Li, *Laser Photonics Rev.*, 2024, 2400791.
85 P. Galajda and P. Ormos, *Appl. Phys. Lett.*, 2001, **78**, 249–251.
86 H. Rubinsztein-Dunlop and M. E. Freise, *Opt. Photonics News*, 2002, **13**, 22–26.

